IEEE Robotics and Automation Letters (RA-L) paper, presented at ICRA 2026, Vienna, Austria. Cite as RA-L paper.

Nezha-X: A Self-Foldable HAUV That Can Launch From a Tube

Dongping Wang, Ziyang Zhang, Zheng Zeng, Lian Lian

***Abstract*—Hybrid aerial underwater vehicles (HAUVs) are developing rapidly with the urgent need for joint air-sea observation missions. This paper proposes a novel HAUV that combines a folding wing mechanism and an underwater thrust system with a centralized tail in an inverted triangle configuration. In addition to ensuring underwater and aerial maneuverability, the design's overall streamlined structure minimizes the drag of underwater movement and is more suitable for working in confined spaces. The hydrodynamic performance of the system was evaluated using computational fluid dynamics (CFD) simulation. The results indicate that the folding wing design effectively reduces underwater motion drag by 41.9%. Additionally, the centralized underwater thrust system located at the tail generates sufficient torque to ensure the underwater maneuverability of the HAUV. Field experiments further validate the vehicle's capability to operate in confined environments, execute complex underwater missions, and maintain stable aerial flight. This study provides valuable insights into the drag reduction of HAUV folding wings and the optimization of thruster configuration.**

***Index Terms*—Hybrid aerial underwater vehicle, foldable wing mechanism, tail-centered triangle thrust system**

I. Introduction

HYBRID aerial underwater vehicles (HAUVs) represent an emerging class of multifunctional robotic platforms capable of seamlessly transitioning between aerial and underwater environments. Their versatility enables a wide range of applications, including ocean exploration, environmental monitoring, and disaster response. However, due to the significant differences in the physical characteristics of under water and air environments, achieving efficient maneuverability, stability, and energy management in two very different physical environments is a major challenge [1].

Most existing HAUV designs have been realized by extending the underwater capabilities of the unmanned aerial vehicles (UAVs) [2], [3]. Specifically, it adopts a sealed design to solve the problem of underwater leakage and is equipped with a power system adapted to the underwater environment movement. Fixed-wing HAUVs have better aerodynamic and endurance characteristics. However, there are strict requirements for speed and attitude in the cross-domain process [4]. Compared with fixed-wing HAUVs, multirotor HAUVs are easy to operate, can accurately hover, and are more convenient for vertical take-off and landing in the cross-domain, which are more suitable for specific application scenarios [5].

Multirotor HAUVs rely on outstretched arms to support their rotors; however, these arms increase the vehicle's surface contact area during underwater operation, resulting in higher hydrodynamic drag. This added drag significantly reduces movement efficiency and increases energy consumption [6]. Furthermore, the extended arms can hinder maneuverability in confined underwater environments, limiting the HAUV's ability to perform complex tasks in such conditions [7]. Folding arms provide an effective solution for reducing underwater drag and enhancing maneuverability in confined spaces, making them a valuable design choice for HAUVs. This technology has been widely adopted in the UAV industry [8], [9], [10] and is increasingly being explored for HAUV applications. The Nezha III employs six motor-driven folding arms, with their fully folded or unfolded states determined by detecting the motor's blocking current. While this design enhances hydrodynamic performance, it also increases the overall weight of the HAUV [11]. To address this issue, the Nezha-F integrates a collapsible, self-deployable arm mechanism actuated by a piston variable buoyancy system (PVBS), reducing underwater resistance by 30.1%. This lightweight design improves efficiency but limits multi-degree-of-freedom underwater movement [12]. Similarly, the Longbow II adopts swept-back folding wings, with a drag reduction effect of 15.3%. Dipper and AquaMAV have similar structures to Longbow II. However, since their wings do not fully fold, the drag reduction effect remains suboptimal [13], [14], [15]. To maximize hydrodynamic efficiency, a fully folding wing design, driven by a single motor, allows the wings to retract completely into the fuselage, significantly reducing drag while minimizing additional weight.

Multirotor HAUVs require additional underwater thrusters for effective submerged operation. However, most of the existing design solutions are to arrange thrusters on the periphery of the HAUVs, which increases spatial requirements and complicates integration with a streamlined body. Combined with the presence of outstretched arms, this configuration leads to increased hydrodynamic drag and energy consumption, while also limiting maneuverability in confined environments [16]. As with many slender underwater vehicles, positioning the thrusters at the rear of the hull is an effective strategy for achieving a streamlined design. However, to enable multi-degree-of-freedom motion control, additional control surfaces such as rudders or vector thrusters are required. Rudders generate steering torque by altering water flow direction, but their effectiveness depends on the vehicle's forward speed, significantly decreasing or even failing at low speeds or when stationary [17]. Vector thrusters, on the other hand, rely on

Manuscript received: December 31, 2024; Revised March 25, 2025; Accepted May 5, 2025.

This paper was recommended for publication by Editor G. Loianno upon evaluation of the Associate Editor and Reviewers' comments. This work was supported by the Oceanic Interdisciplinary Program of Shanghai Jiao Tong University(project number SL2022ZD106 and SL2023ZD206).(Corresponding author: Zheng Zeng, Ziyang Zhang.)

The authors are with State Key Laboratory of Submarine Geoscience ;Key Laboratory of Polar Ecosystem and Climate Change, Ministry of Education; and School of Oceanography, Shanghai Jiao Tong University, China. wangdongping@sjtu.edu.cn; ziyang_zhang@sjtu.edu.cn; zheng.zeng@sjtu.edu.cn; llian@sjtu.edu.cn

Digital Object Identifier (DOI): see top of this page.

IEEE Robotics and Automation Letters (RA-L) paper, presented at ICRA 2026, Vienna, Austria. Cite as RA-L paper.

TABLE I
COMPARISON OF SEVERAL FOLDING ARM HAUVS

Prototypes	Type	Folding Mode	Underwater thrust system	Drag reducing effect	Weight
Nezha-III[11]	Vertical take-off and landing	Folding arm	Pneumatic buoyancy system	-	18kg
Nezha-F[12]	Quadrotor	Folding arm	PVBS	30.1%	1.25kg
Longbow II[13]	Fixed-wing	Swept-back wing	Single propeller+Rudder	15.3%	13.3kg
Dipper[14]	Fixed-wing	Swept-back wing	Single propeller+Rudder	-	3.1kg
AquaMAV[15]	Fixed-wing	Swept-back wing	Water jet	-	0.2kg
Nezha-X	Quadrotor	Folding wing	Tail concentrated inverted triangle propellers	41.9%	3kg

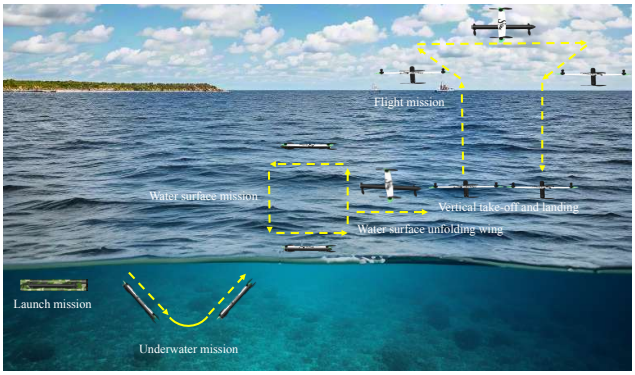

Fig. 1. Schematic diagram of all working mode, including underwater motion, water surface motion, water surface unfolding wing and air motion.

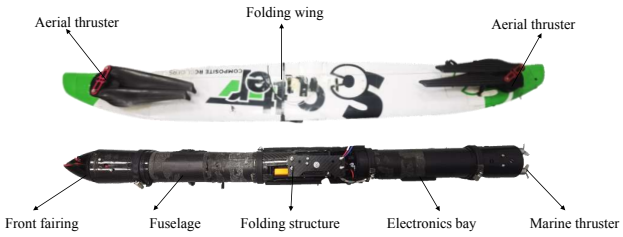

Fig. 2. Main components of Nezha-X design.

external servo motors for actuation, but these motors are prone to corrosion and present sealing challenges in practical applications [18]. A centralized multi-thruster configuration at the vehicle's tail offers an alternative approach, optimizing underwater maneuverability through precise thrust distribution while maintaining a streamlined design.

This paper presents the design of Nezha-X, a HAUV that integrates a folding wing mechanism with a centralized tail-mounted thrust system in an inverted triangle configuration. The folding wing design significantly reduces underwater drag by 41.9% in its folded state, enabling the vehicle to maintain a low-drag profile for efficient underwater operations. When unfolded, the wings facilitate vertical takeoff from the water, ensuring a stable transition between domains. The inverted triangle thrust system is fully integrated into the fuselage, providing essential underwater maneuverability while combining with the folding wing design contributing to the streamlined structure of Nezha-X. This design minimizes cross-sectional

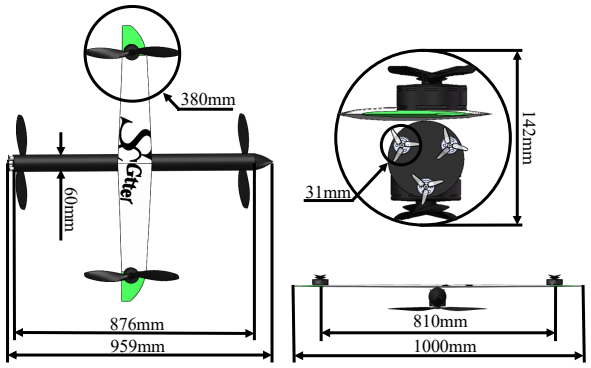

Fig. 3. Main dimensions of Nezha-X geometry design.

area and overall drag, enhancing adaptability for operations in confined spaces.

A comparative summary of existing folding arm HAUV prototypes is presented in Table I, with Nezha-X included at the bottom as introduced in this study. It is worth noting that the resistance reduction values reported in the table were all obtained through the CFD method. It can be seen that the drag reduction effect of HAUV is maximized. Fig. 1 illustrates the schematic of a full-domain experimental task performed by Nezha-X. In this experiment, Nezha-X initiates movement from a narrow tube, enters the water, and executes ascent and dive maneuvers. It then follows a rectangular trajectory along the water surface before undergoing wing unfolding. In its unfolded state, Nezha-X takes off from the water, performs a triangular flight trajectory in the air, and subsequently returns to the water surface for landing.

The remainder of this letter is organized as follows. Section II details the structural design and electronic system of Nezha-X. Section III defines the coordinate system, presents the kinematic parameters, and outlines the corresponding control strategy. Section IV discusses fluid simulation of drag and vertical plane maneuverability. Section V describes the full-domain field experiments conducted to validate the proposed design. Finally, Section VI concludes the letter.

II. PROTOTYPE VEHICLE DESIGN

A. Configuration Overview

The Nezha-X is composed of a carbon fiber fuselage, a folding wing mechanism, and integrated air and underwater

IEEE Robotics and Automation Letters (RA-L) paper, presented at ICRA 2026, Vienna, Austria. Cite as RA-L paper.

thrust systems, as illustrated in Fig. 2. The fuselage consists of two carbon fiber tubes, with both ends sealed using nylon-reinforced end caps and O-rings. These tubes are connected via a hoop structure, forming a robust and integrated frame. The folding wing is reinforced with carbon fiber tubes, which not only provides a certain buoyancy but also significantly increases the water surface contact area. This makes the buoyancy distribution of Nezha-X more uniform and the stability better. The wing is closely integrated with the rotating motor located at the center of the fuselage. This mechanism enables Nezha-X to transition between configurations: in the folded state, it minimizes cross-sectional area and reduces underwater drag, while in the unfolded state, it facilitates surface takeoff for seamless aerial transition. The aerial thrust system adopts a cross-shaped layout, with thrusters distributed across the fuselage and wings. The underwater thrust system features a tail-centered inverted triangle configuration, where yaw and pitch torques are controlled through differential thrust from three thrusters. This scheme ensures the underwater maneuverability of the Nezha-X, effectively avoids the extension of the fuselage length, and minimizes the cross-sectional area of the fuselage at the same time, thereby significantly reducing the resistance during underwater movement.

The Nezha-X has a total weight of 3 kg, with its wing design centered around the fuselage. The 5000 mAh 6s LiPo battery powering the aerial motor is positioned at the front of the fuselage, while a 2200 mAh 3s LiPo battery and an electronics compartment are located at the rear to supply power to the marine motor. This arrangement ensures a balanced distribution of mass throughout the fuselage. The positions of the center of gravity (CG) and center of buoyancy (CB) exhibit minimal variation in both the folded and unfolded configurations. The design aligns the CB vertically above the CG, ensuring dynamic stability and balance during underwater operations in both configurations. Compared with the change of CG and CB before and after the folded wing, the difference of moment of inertia is more significant. In the unfolded state, the moment of inertia of Nezha-X is [0.0547,0.1840,0.2359]kg·m², whereas in the folded configuration, it changes to [0.0024,0.2364,0.2361] kg·m². The reduction in roll moment of inertia after folding increases Nezha-X's susceptibility to rolling motions. Conversely, the increase in the pitch moment of inertia makes the pitch change more difficult.

The full fuselage length of the Nezha-X is 959 mm, with the main fuselage measuring 876 mm in length and a diameter of 60 mm. The wingspan extends to 1,000 mm, and the spacing between the two aerial thrusters is 810 mm. The aerial propeller has a diameter of 380 mm, while the underwater propeller measures 31 mm in diameter. The overall fuselage envelope has a diameter of 142 mm, as shown in Fig. 3.

B. Avionics System

A dual microcontroller architecture is used to control the movement in water and air. The circuit design includes two parts: flight controller and underwater controller, which correspond to the working requirements of different environments, respectively, as shown in Fig. 4.

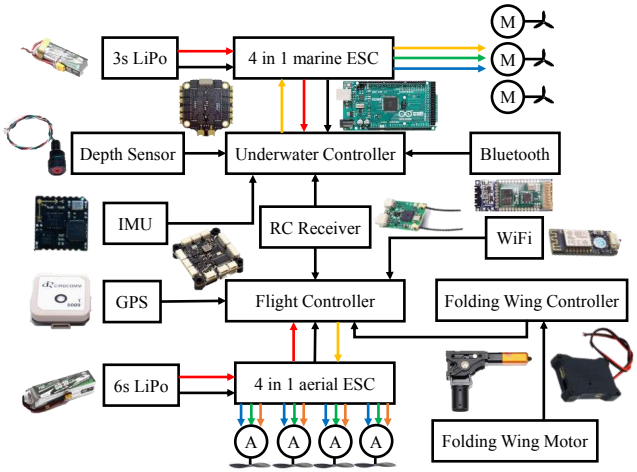

Fig. 4. Avionics system diagram. A dual-microcontroller architecture is used to control the motion underwater and in the air.

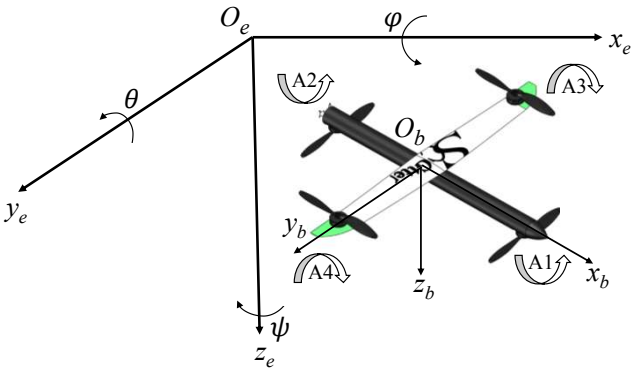

Fig. 5. Model of Nezha-X with the marks on the coordinate systems and obverse directions.

The flight controller is based on standard quadcopter firmware and integrates several key components, including a GPS module, a signal receiver, a WiFi module for communication with the ground station, an SD memory card, and a separate control module for managing the folding wing mechanism. The flight controller is powered by a 6s LiPo battery, with power supplied through a battery eliminator circuit (BEC) integrated into the four-in-one electronic speed controller (ESC). The underwater controller incorporates an independent signal receiver, an attitude sensor, and a depth sensor (MS5837), which communicate with the controller via USART and I2C protocols, respectively. It operates based on a pre-programmed algorithm uploaded through the HC-06 Bluetooth module and records voyage data by interacting with the SD memory card via the SPI protocol. The underwater controller is powered by a 3s LiPo battery, with power supplied through the BEC in the four-in-one ESC.

III. Motion Definition and Control Strategy

A. Coordinate system and motion parameter definition

In order to study the motion of Nezha-X and determine the position and direction of the motion, the following two coordinate systems are established, as shown in Fig. 5. $O_e - x_e y_e z_e$

IEEE Robotics and Automation Letters (RA-L) paper, presented at ICRA 2026, Vienna, Austria. Cite as RA-L paper.

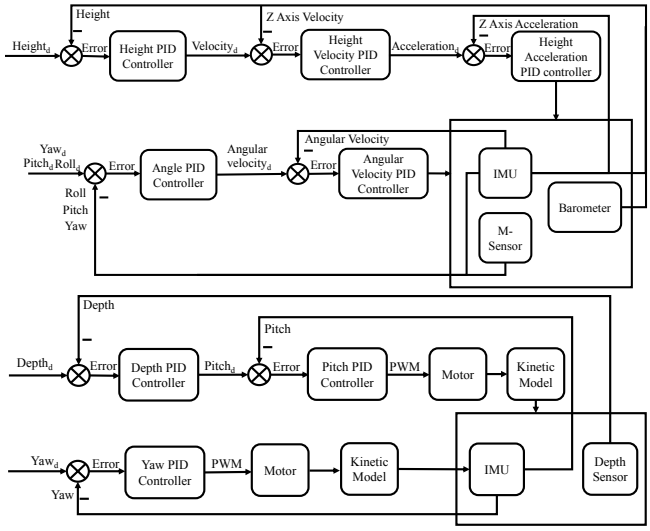

Fig. 6. Schematic diagram of control framework.

is the earth coordinate system, which is used to represent the spatial position and direction of Nezha-X and $O_b - x_b y_b z_b$ is the body-fixed coordinate system, which is used to represent the velocity of Nezha-X. The position and attitude of the Nezha-X motion can be expressed by the position $[x\ y\ z]^T$ of the coordinate origin of the body-fixed coordinate system $O_b - x_b y_b z_b$ in the earth coordinate system $O_e - x_e y_e z_e$ and the direction angle $[\varphi\ \theta\ \psi]^T$. The vehicle travels at linear velocity V with a projection $V = [u\ v\ w]^T$ in the coordinate system, and rotates at angular velocity Ω with a projection of $\Omega = [p\ q\ r]^T$.

B. control strategy

Nezha-X employs distinct control strategies for air and underwater operations to meet the requirements of multi-environment tasks, as illustrated in Fig. 6. In the aerial mode, altitude control follows a three-ring control structure: the outer ring tracks altitude, the middle ring monitors the Z-axis velocity, and the inner ring tracks the Z-axis acceleration. Control signals are progressively output to ensure precise altitude regulation. Attitude control utilizes a two-ring control scheme, with the outer ring tracking the attitude angle and the inner ring monitoring angular velocity to maintain attitude stability. In underwater mode, yaw control is implemented using a single-loop control system, where a PWM signal is generated based on the yaw angle error to adjust the speeds of the left and right thrusters for steering. Depth control adopts a two-ring structure: the outer ring controls depth and outputs the desired pitch angle, while the inner ring adjusts the speeds of the upper and lower thrusters to facilitate ascent or dive.

IV. Fluid Simulation Verification

A. Drag of folded and unfolded wing underwater

The drag characteristics of the folded and unfolded wing in underwater motion were quantitatively evaluated by CFD simulation. In the simulation process, a simplified geometric

TABLE II
THREE MESHES WITH DIFFERENT DENSITIES.

Mesh density	Total number of cells	Drag	Lift
Coarse	2821542	3.08	11.15
Medium	4485844	3.10	11.31
Dense	8883908	3.11	11.30

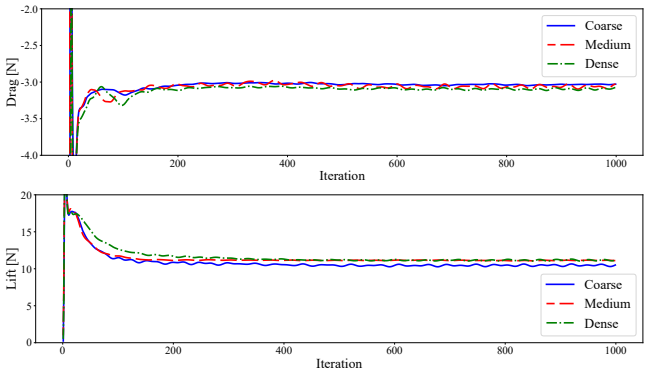

Fig. 7. Mesh independence study result.

model was utilized. The model retained only the fuselage, wings, and motors to focus on the primary structural elements.

The Reynolds Average Navier-Stokes (RANS) equation is used as the governing equation, the SST $k - w$ turbulence model is adopted [19], and the finite volume method is used to discretely solve the governing equation. The computational domain is set as a cuboid region where the entry position is 2L from the front of the fuselage, the exit position is 5L from the rear of the fuselage, and the top, bottom, left, and right boundaries are 2L from the fuselage (where L is the length of the fuselage). The simulation conditions set the inflow velocity to 1 m/s. In terms of mesh partitioning, prism layer mesher are used near the Nezha-X surface to accurately capture the boundary layer characteristics, while trimmed cell mesher are used in other areas, and trimmer wake refinement is performed to improve the accuracy of the flow field analysis and greatly enhance the reliability of the simulation results. Considering the computational resources and the accuracy of the results, the verification of mesh independence was carried out. Three computational models with different numbers of meshes, coarse, medium and dense, were selected to numerically simulate the Nezha-X flow field, as shown in Table II. The results of the mesh independence validation for the drag and lift of the unfolded wing are presented in Fig. 7. The findings indicate a significant discrepancy in the results obtained using the coarse mesh, whereas the differences between the medium and dense meshes are minimal. Considering both computational accuracy and cost, the medium-density mesh was selected for the final calculations.

The drag force data were collected for the two models. The simulation results as shown in Fig. 8. The drag of the folded wing is 1.80 N when moving in water. In contrast, the unfolded wing configuration has a drag of 3.10 N. Compared to the unfolded wing configuration, the folded wing config-

IEEE Robotics and Automation Letters (RA-L) paper, presented at ICRA 2026, Vienna, Austria. Cite as RA-L paper.

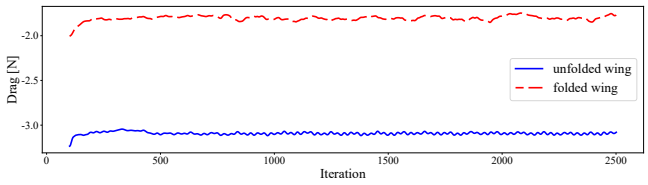

Fig. 8. CFD simulation drag diagram of folded and unfolded wing underwater.

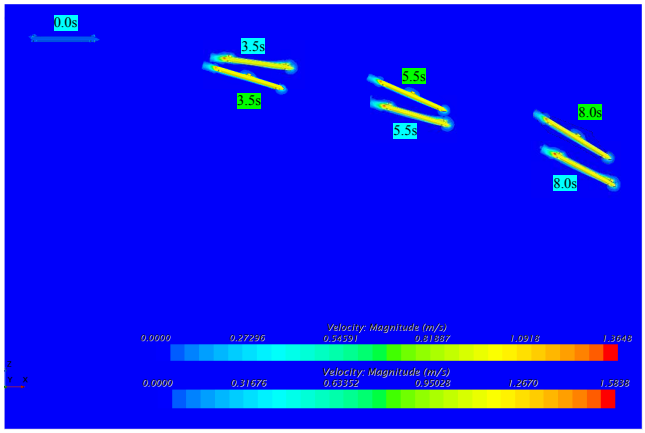

Fig. 9. Fixed thrust performance of folded and unfolded wing in the vertical plane.

uration has a smaller frontal flow area and reduces drag by 41.9%. The results show that folding wings have a good drag reduction effect, providing a new approach for underwater drag reduction.

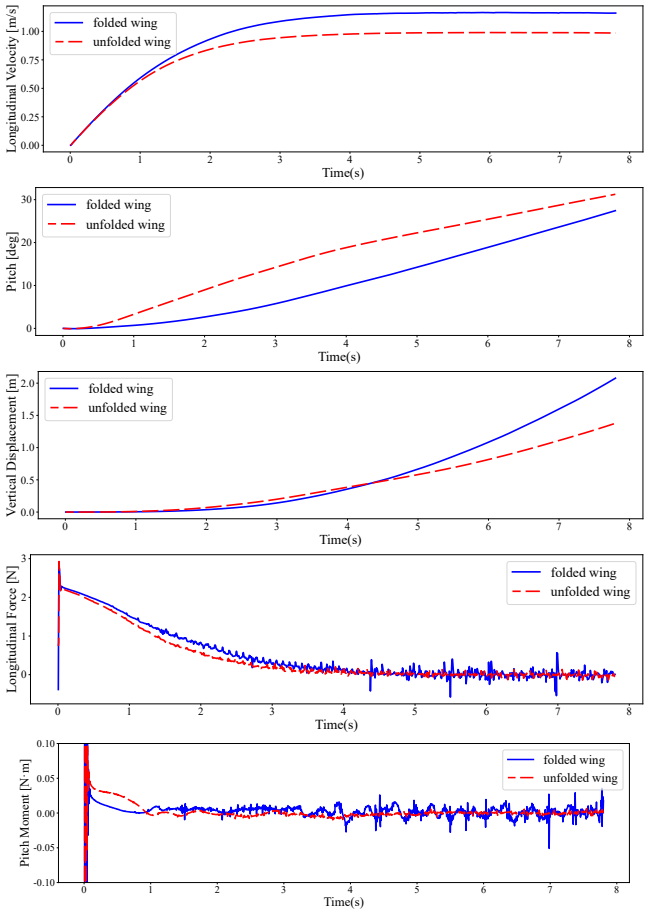

Fig. 10. The velocity, attitude angle, position and force (moment) change curves of folded and unfolded wing in the vertical plane during the simulation.

B. Fixed thrust performance in vertical plane

An inverted triangular thrust configuration with a concentrated tail ensures a streamlined Nezha-X design. In order to verify that this thrust configuration can generate enough torque to realize the free movement of the Nezha-X underwater. Based on the simplified geometry model, a CFD simulation of the vertical movement of the Nezha-X was carried out. Additionally, simulations were conducted for both the folded and unfolded wing configurations of Nezha-X to assess its hydrodynamic performance. Commercial software STAR-CCM+ was used for CFD simulation. Based on RANS equation, constant density, implicit unsteady solution method and SST $k-w$ turbulence model were selected to optimize the prediction accuracy of hydrodynamic viscosity. Considering the coupled motion characteristics of Nezha-X, the overset grid and dynamic fluid-body interaction (DFBI) methods are used in the simulation. The computational domain consists of two main regions: a large static background mesh to simulate the entire flow field, and a dynamic mesh region to translate and rotate with Nezha-X.

The vertical motion of the Nezha-X is provided by a fixed thrust defined at the rear of the fuselage in a circular array arrangement (no additional pitching moment is defined). The fixed thrust not only provides forward thrust for the Nezha-X, but also produces pitching torque due to the non-coincidence of its application point and CG, thus driving the Nezha-X to dive. In addition to the individual thrust, the Nezha-X is also subject to the combined action of gravity and hydrodynamic forces during movement. Therefore, the resultant force and the resultant moment subjected to Nezha-X can be expressed as the following mathematical expression:

$$\begin{aligned} F &= \left(F_f + F_g + \sum F_{ud}\right) \\ M &= \left(M_f + \sum M_{ud}\right) \end{aligned} \tag{1}$$

where F_f is the hydrodynamic force, F_g is the gravity, F_{ud} is the user-defined external force, M_f is the hydrodynamic moment and M_{ud} is the user-defined external moment.

$$\begin{aligned} F_{ud} &= [T_{M1} + T_{M2} + T_{M3},\ 0,\ 0]^T \\ M_{ud} &= r_{M1} \times [T_{M1},\ 0,\ 0]^T + r_{M2} \times [T_{M2},\ 0,\ 0]^T + \\ &\quad r_{M3} \times [T_{M3},\ 0,\ 0]^T \end{aligned} \tag{2}$$

where T_{M1} T_{M2} T_{M3} are three thrust forces in the tail, the size of which is 2.5 N (determined by the results of the propeller thrust experiment), in which the upper two thrust forces are in the positive direction of the x-axis and the next thrust is in the opposite direction. r_{M1} r_{M2} r_{M3} are the position coordinates of the three thrusts.

Fig. 9 shows the motion trajectory of Nezha-X under two working conditions of folded and unfolded wing in the simu-

IEEE Robotics and Automation Letters (RA-L) paper, presented at ICRA 2026, Vienna, Austria. Cite as RA-L paper.

Fig. 11. The process diagram of launch experiment.

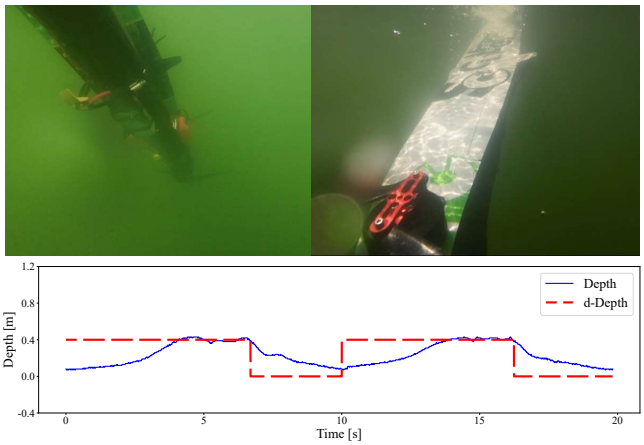

Fig. 12. Underwater ascent and dive experiment and data presentation.

lation process. Fig. 10 presents the time-varying curves of velocity, attitude angle, position, and force (moment) under two operational conditions, illustrating the dynamic characteristics of Nezha-X in different configurations. In the initial phase of motion, the unfolded wing configuration exhibits a greater diving depth and a larger pitch angle. This behavior is likely due to the lift force acting at the wing's center of pressure, generating a bowing moment that causes the HAUV to pitch downward. At low initial speeds, where drag is minimal, the significant lift force of the unfolded wing configuration dominates attitude adjustment, facilitating a rapid dive. In contrast, the folded wing configuration experiences lower lift, resulting in a slower dive and a more gradual increase in pitch angle. In the middle and late stages of movement, as the motion progresses, increasing velocity leads to a significant rise in hydrodynamic drag, reducing acceleration and stabilizing speed. The folded wing configuration, characterized by lower drag, achieves a higher steady-state velocity. The higher speed translates into greater vertical displacement through pitch angle adjustment.

A comprehensive analysis indicates that the fixed thrust system, arranged in a circular array at the fuselage tail, generates sufficient pitching moment to support HAUV diving. While the unfolded wing configuration initially benefits from lift-induced rapid diving, its high drag constrains continuous speed growth. Conversely, the folded wing configuration, with reduced drag, accumulates higher speeds in later stages, ultimately achieving greater depth. Compared to the unfolded wing state, the folded wing configuration offers superior diving depth, lower drag in underwater motion, higher velocity, and extended endurance, making it advantageous for underwater operational applications.

V. EXPERIMENTS

A. Launch experiment

The Nezha-X has a small cross-sectional area and is capable of moving through confined spaces during underwater operation. In order to verify the Nezha-X's ability to move in a confined environment, the launch experiment was conducted. The experiment was conducted in a controlled pool environment, where the Nezha-X was first deployed in a 160 mm diameter tube and the marine motor was started by remote control to achieve rapid launch from the tube. The experimental results are shown in Fig. 11, which shows that the Nezha-X successfully completed the process of launching the tube in 3 s, verifying its maneuverability and operability in a confined space. The experimental results provide an important experimental basis for the deployment and application of HAUV in complex confined environments.

B. Underwater depth experiment

Stable depth holding performance is the basis for the application of HAUV in underwater operation. The Nezha-X underwater depth experiment was conducted in Qiandao Lake, Zhejiang Province, China. The total duration of the experiment was 20 s, the target depth was set to 0.4 m, and two stages of depth-holding operations were carried out, each lasting 10 s. In each cycle, Nezha-X completes the dive and depth-holding process within 7 seconds, after which the target depth is automatically set to 0 m for ascent. The experimental results, as shown in Fig. 12, demonstrate the system's rapid response capability in dynamic experiments. Nezha-X is able to perform stable ascent and dive in continuous cycles and maintain a steady linear cruise at the designated depth. The average depth error during the depth-holding phase is less than 0.1 m, indicating high control precision and system stability. These findings confirm that Nezha-X meets the practical requirements for underwater operations.

C. Straight line and steering experiment

Straight line and steering ability is the core index of HAUV motion control performance. To evaluate its motion performance, the surface rectangular motion experiment was conducted in Zhiyuan Lake, Shanghai Jiao Tong University (SJTU), China. During the experiment, Nezha-X followed a predefined heading sequence of 31.1°, -58.9°, -148.9°, and 121.1° from the starting point, while real time attitude data

IEEE Robotics and Automation Letters (RA-L) paper, presented at ICRA 2026, Vienna, Austria. Cite as RA-L paper.

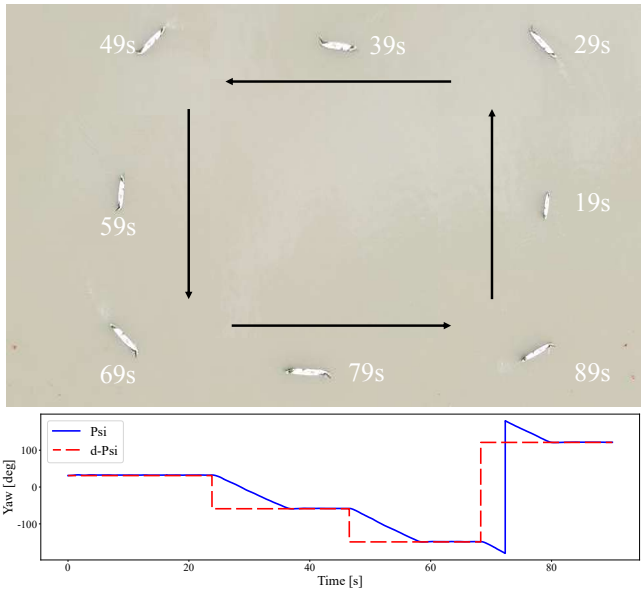

Fig. 13. Underwater straight line and steering experiment and data presentation.

Fig. 14. Diagram of the unfolding process of the wing.

were recorded to assess its heading control performance and path-tracking capability. The experimental results, presented in Fig. 13, indicate that although the HAUV exhibits slight deviations during turns, it maintains high stability along straight segments, with heading errors consistently within 2°. These results demonstrate the HAUV's effective heading control capability and validate its feasibility for executing rectangular path tracking in surface environments, providing a foundation for more complex task execution.

D. Water surface wing unfolding experiment

The folding wing mechanism is critical for enabling Nezha-X to transition from an underwater state to aerial flight. A servomotor drives the folding system, allowing the wings

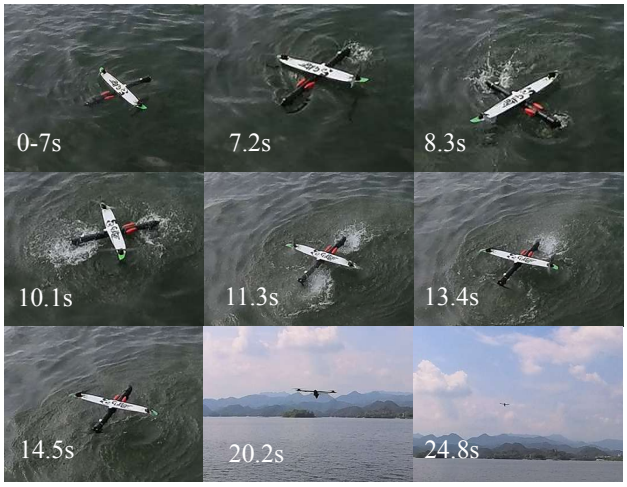

Fig. 15. Sequence diagram of the cross-domain locomotion.

to transition between folded and unfolded states within a maximum range of 90°. The controller receives remote control signals to precisely regulate the movement of servomotor. To enhance system safety, the control system incorporates both current and time protection mechanisms; if either is triggered, the controller ceases operation to prevent equipment damage. A wing folding experiment was conducted at Qiandao Lake, Zhejiang Province, China, to assess the reliability and performance of the system. The experimental results, shown in Fig. 14, indicate that the average folding time is 9 seconds, meeting the requirement for rapid response. Additionally, the wings consistently reached the predefined target positions with high precision, demonstrating the system's accuracy and reliability. No structural deformation or damage was observed during repeated trials, further validating the structural stability and folding performance. These results confirm that the folding wing system satisfies the practical application requirements for cross-domain vehicles.

E. Cross-domain experiment

Stable cross-domain capability is a core feature of the HAUV. The air-water transition experiment of Nezha-X was conducted at Qiandao Lake, Zhejiang Province, China, as shown in Fig. 15, with a partial flight log presented in Fig. 16. The cross-domain flight process can be divided into several phases. Phase 0–7 s: Nezha-X's wing motors (A1 and A2) remain above water, while the fuselage motors (A3 and A4) are submerged. The throttle is set to its lowest level, resulting in minimal voltage drop and current output. Due to water surface disturbances, the pitch and roll angles oscillate around 0°. Phase 7–11 s: The throttle is gradually increased to adjust Nezha-X's heading, and the motors transition into an idle state. Phase 11–14 s: The throttle is further increased, causing A1 and A2 to operate at higher speeds on the water surface, while A3 and A4 experience lower speeds due to increased underwater drag. At this stage, Nezha-X's attitude changes, and energy consumption rises significantly, with a maximum voltage drop of 2.3 V and a peak current of 50 A. The flight controller dynamically adjusts motor speeds to stabilize the

IEEE Robotics and Automation Letters (RA-L) paper, presented at ICRA 2026, Vienna, Austria. Cite as RA-L paper.

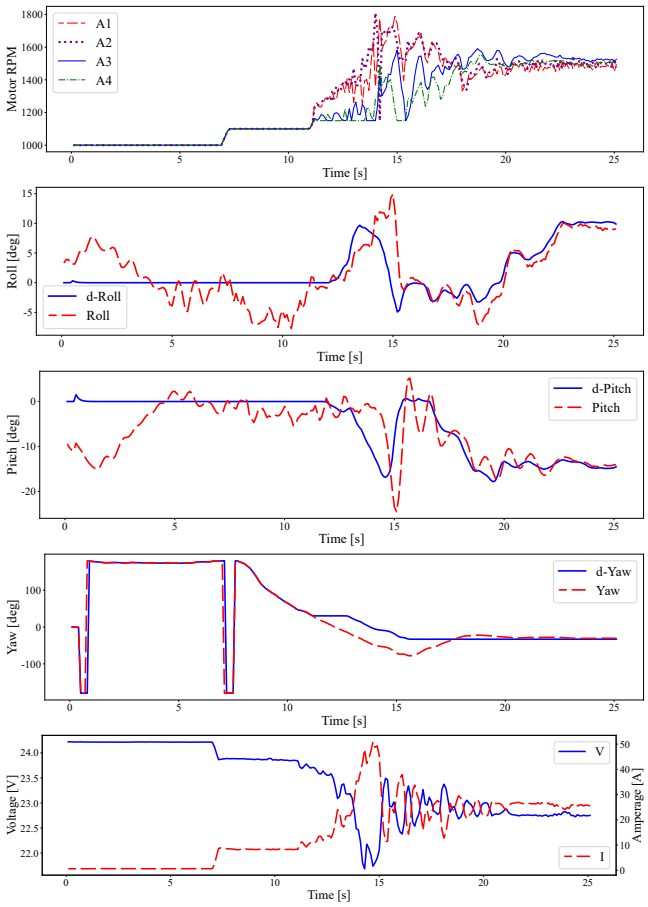

Fig. 16. Flight logs including attitude, power, and RPM.

vehicle. Post 14 s: Nezha-X fully exits the water, achieving stable motor speeds. The four motors operate at approximately 50% of the speed threshold, the roll and yaw angles stabilize, and energy consumption decreases to the normal flight level. Experimental results demonstrate that Nezha-X exhibits high attitude control precision during the cross-domain transition and responds rapidly to control commands. Despite minor attitude fluctuations near the water surface, the overall transition process remains highly stable. These findings validate the feasibility of Nezha-X in water-air interface switching and establish a foundation for executing complex cross-domain missions.

VI. Conclusion

The Nezha-X proposed in this paper combines the inverted triangle underwater thrust system with the folded wing structure. Simulation and field tests prove that, on the premise of ensuring stable cross-domain transition and not losing the basic maneuvering performance in underwater and air environments, Nezha-X can maintain a streamlined shape by minimizing the cross-sectional area. This results in 41.9% maximum drag reduction in the full configuration and the ability to use in confined spaces. The results confirm the feasibility and reliability of the proposed design, laying a foundation for future advancements in cross-domain vehicle technology.

However, the current research has not yet achieved fixed-wing flight due to challenges in integrating the necessary underwater propulsion systems. Future research directions could focus on optimizing the weight and aerodynamic efficiency of the HAUV's wings, incorporating aileron, empennage and folding propeller, developing a tiltrotor or quadplane vertical take-off and landing (VTOL) design while retaining the current folding wing structure.

References

[1] Z. Zeng, C. Lyu, Y. Bi, Y. Jin, D. Lu, and L. Lian, "Review of hybrid aerial underwater vehicle: Cross-domain mobility and transitions control," *Ocean Eng.*, vol. 248, 2022.

[2] Z. Bodó and B. Lantos, "Modeling and control of fixed wing uavs," in *SACI - IEEE Int. Symp. Appl. Comput. Intell. Informatics, Proc.*, 2019, pp. 332–337.

[3] S. K. Phang, S. Zeeshan Ahmed, and M. R. Abdul Hamid, "Design, dynamics modelling and control of a h-shape multi-rotor system for indoor navigation," in *Int. Conf. Unmanned Veh. Syst.-Oman, UVS*, 2019, pp. 1–6.

[4] Y. Jin, Z. Zeng, and L. Lian, "Nezha-seadart: A tail-sitting fixed-wing vertical takeoff and landing hybrid aerial underwater vehicle," *J. Field Robot.*, vol. 42, no. 1, pp. 137–152, 2024.

[5] Y. Liu, C. Li, J. Li, Z. Lin, W. Meng, and F. Zhang, "Wukong: Design, modeling and control of a compact flexible hybrid aerial-aquatic vehicle," *IEEE Robot. Autom. Lett.*, pp. 1–8, 2024.

[6] L. Yan, A. Cao, X. Zhu, H. Ding, H. Lu, and G. Chen, "Design and analysis of a novel hybrid aerial underwater vehicle with foldable wings," in *Proc. Chin. Control Decis. Conf., CCDC*, 2024, pp. 361–366.

[7] A. Vyas, R. P. N. Sivadasan, A. Molawade, T. Ranganathan, and A. Thondiyath, *Modelling and Dynamic Analysis of a Novel Hybrid Aerial - Underwater Robot - Acutus*, ser. Proc. IEEE OCEANS., 2019.

[8] H. Yu, J. Lu, J. Gao, S. Cao, L. Yu, and L. Wu, "Conceptual design and test of a tilting quadrotor morphing unmanned aerial vehicle with adaptive foldable wings," in *Lect. Notes Electr. Eng.*, 2021, pp. 945–954.

[9] D. Falanga, K. Kleber, S. Mintchev, D. Floreano, and D. Scaramuzza, "The foldable drone: A morphing quadrotor that can squeeze and fly," *IEEE Robot. Autom. Lett.*, vol. 4, no. 2, pp. 209–216, 2018.

[10] S. Hu, Y. Li, T. Gao, and Q. Wang, "Design of a foldable multirotor for rapid deployment in complex environments," in *Lect. Notes Electr. Eng.*, 2023, pp. 237–248.

[11] D. Lu, C. Xiong, H. Zhou, C. Lyu, R. Hu, C. Yu, Z. Zeng, and L. Lian, "Design, fabrication, and characterization of a multimodal hybrid aerial underwater vehicle," *Ocean Eng.*, vol. 219, p. 108324, 2021.

[12] Y. Bai, Y. Jin, C. Liu, Z. Zeng, and L. Lian, "Nezha-f: Design and analysis of a foldable and self-deployable hauv," *IEEE Robot. Autom. Lett.*, vol. 8, no. 4, pp. 2309–2316, 2023.

[13] X. Sun, J. Cao, Y. Li, and B. Wang, "Design and field test of a foldable wing unmanned aerial–underwater vehicle," *J. Field Robot.*, vol. 41, no. 2, pp. 347–373, 2023.

[14] F. M. Rockenbauer, S. Jeger, L. Beltran, M. Berger, M. Harms, N. Kaufmann, M. Rauch, M. Reinders, N. R. Lawrance, T. Stastny *et al.*, "Dipper: A dynamically transitioning aerial-aquatic unmanned vehicle." in *Proc. Robot. Sci. Syst.*, vol. 2021, 2021, pp. 12–16.

[15] S. Robert, O. A. Alejandro, and K. Mirko, "Wind and water tunnel testing of a morphing aquatic micro air vehicle." *Interface focus*, vol. 7, no. 1, p. 20160085, 2017.

[16] Y. Jin, Y. Bi, C. Lyu, Y. Bai, Z. Zeng, and L. Lian, "Nezha-iv: A hybrid aerial underwater vehicle in real ocean environments," *J. Field Robot.*, vol. 41, no. 2, pp. 420–442, 2024.

[17] H. Xia, P. Wang, Z. Jin, X. An, and Y. Ding, "Maneuverability analysis of thrust vectoring ducted propeller with deflector," *Ocean Eng.*, vol. 213, p. 107614, 2020.

[18] Y. Li, P. Gao, Y. Wang, and C. Ren, "The implementation and evaluation of a multi-dofs coanda-effect jet device for underwater robots," *Appl. Ocean Res.*, vol. 108, p. 102545, 2021.

[19] J. Steelant and E. Dick, "Modeling of laminar-turbulent transition for high freestream turbulence," *J. Fluids Eng.-Trans. ASME*, vol. 123, no. 1, pp. 22–30, 2001.